Microchimica Acta (2023) 190:57
https://doi.org/10.1007/s00604-023-05645-x

ORIGINAL PAPER

Colorimetric and photothermal dual-mode lateral flow immunoassay based on Au-Fe_3O_4 multifunctional nanoparticles for detection of *Salmonella typhimurium*

Cong-Ying Wen[1] · Ling-Jin Zhao[1] · Ying Wang[1] · Kun Wang[1] · Hui-Wen Li[1] · Xiang Li[1] · Min Zi[1] · Jing-Bin Zeng[1]

Received: 24 October 2022 / Accepted: 2 January 2023 / Published online: 18 January 2023

Abstract

Au-Fe_3O_4 multifunctional nanoparticles (NPs) were synthesized and integrated with lateral flow immunoassay (LFIA) for dual-mode detection of *Salmonella typhimurium*. The Au-Fe_3O_4 NPs not only combined excellent local surface plasmon resonance characteristics and superparamagnetic properties, but also exhibited good photothermal effect. In the detection, antibody-conjugated Au-Fe_3O_4 NPs first captured *S. typhimurium* from complex matrix, which was then loaded on the LFIA strip and trapped by the T-line. By observing the color bands with the naked eyes, qualitative detection was performed free of instrument. By measuring the photothermal signal, quantification was achieved with a portable infrared thermal camera. The introduction of magnetic separation achieved the enrichment and purification of target bacteria, thus enhancing the detection sensitivity and reducing interference. This dual-mode LFIA achieved a visual detection limit of 5×10^5 CFU/mL and a photothermal detection limit of 5×10^4 CFU/mL. Compared with traditional Au-based LFIA, this dual-mode LFIA increased the detection sensitivity by 2 orders of magnitude and could be directly applied to unprocessed milk sample. Besides, this dual-mode LFIA showed good reproducibility and specificity. The intra-assay and inter-assay variation coefficients were 3.0% and 7.9%, and with this dual-mode LFIA, other bacteria hardly produced distinguishable signals. Thus, the Au-Fe_3O_4 NPs-based LFIA has potential to increase the efficiency of pandemic prevention and control.

Keywords Magnetic separation · Bacteria · LFIA strip

Introduction

Food safety problem continues to present a major threat to human health and social security. According to the World Health Organization, foodborne diseases cause ca. 600 million to fall ill, 420,000 to die, and hundreds of billions of US$ lost years, which severely threaten human health and impede socioeconomic development [1]. To effectively reduce the above losses, early and reliable detection plays a key role [2, 3]. *Salmonella*, as one of the most common foodborne pathogens, affects millions of people annually, sometimes with severe and fatal outcomes, and thus has always been an important monitoring target for food safety [1, 4, 5]. Currently, the main methods used in practice are culture-based assays, polymerase chain reaction (PCR) analyses, and enzyme-linked immunosorbent assay (ELISA). Culture-based assays are the gold standard method owing to their high accuracy but limited by time-consuming and labor-intensive manipulation. PCR has high sensitivity but requires sophisticated instruments and skilled technical staffs, restricting its applications. ELISA simplifies the detection procedure to a certain degree, yet it still suffers from the limitations like relatively low sensitivity and time consumption [6–9]. Thus, these methods cannot be applied to on-site detection or large-scale screening, which seriously restricts the efficiency of pandemic prevention and control.

Lateral flow immunoassay (LFIA) has shown great promise in on-site instant diagnosis, due to its enormous advantages including high speed, low cost, portability, convenience, free of instrument or skilled staff [10–12]. The most successful application of LFIA is the pregnancy test strips,

✉ Cong-Ying Wen
flcyxt@163.com

✉ Jing-Bin Zeng
xmuzjb@163.com

[1] College of Chemistry and Chemical Engineering, China University of Petroleum (East China), Qingdao 266580, People's Republic of China

which change hospital-dependent detection to rapid home self-testing, thereby highly improving diagnosis efficiency and reducing costs [13, 14]. However, applying traditional LFIA to bacteria detection faces three main bottleneck problems. One is the low sensitivity which may result in missed detection. The second is that it is a yes-or-no diagnosis which cannot provide accurate quantitative information for guiding therapy. The third is that it cannot be directly applied to complex matrix which must be diluted before flowing on the strips, and this seriously limits its practical application due to the fact that many pathogenic bacteria usually exist in complex biological samples at very low concentration [10, 15–17]. The key reason that induces the above drawbacks is that traditional LFIA mainly uses gold nanoparticles (NPs) as reporters.

In recent decades, researchers have been trying to develop various nanomaterials as new reporters to replace gold NPs, such as dyed beads, fluorescent NPs, surface-enhanced Raman scattering-active nanomaterials, and carbon nanomaterials, which have increased the sensitivity and realized quantitative detection [18–21]. Nevertheless, with these reporters, dilution is still necessary for complex samples, which may lower the sensitivity in practical detection. Magnetic NPs may be promising alternative reporters to solve this problem. Magnetic NPs can effectively capture, separate, and concentrate target bacteria from a large volume of sample into a small volume of buffer under an external magnetic field, thereby realizing purification and enrichment [22–25]. Some works have confirmed the superiority of magnetic reporters in the LFIA. For example, Hwang et al. coated Au NPs on Fe_3O_4 nanoclusters, with which sensitive detection of *Salmonella* in milk was achieved [26]. As other examples, Hu et al. and Wang et al., respectively, prepared fluorescent-magnetic nanocomposites by repeated assembling methods and developed multimodal LFIAs for *Salmonella* and *S. pneumoniae* detection in milk, serum, or whole blood samples [27, 28]. The above magnetic-colorimetric reporters-based LFIA exhibited obvious advantages over conventional LFIA, yet the preparation of the reporters generally involved more than two kinds of nanoparticles and their assembly, which were complicated and time/labor-consuming.

In our previous work, we proposed a universal seed-mediated growth method to directly synthesize hydrophilic coinage metal/iron oxide (M-Fe_3O_4) heterodimer NPs, such as Ag-Fe_3O_4, Pd-Fe_3O_4, and AgPt-Fe_3O_4 [29–32]. These M-Fe_3O_4 NPs not only combined multiple functions, but also showed improved bio-modifiability and water compatibility with good tunability. Herein, based on our previous work, we directly synthesized Au-Fe_3O_4 heterodimer NPs, avoiding the assembly of two kinds of NPs, which was much more convenient and time-saving. The Au-Fe_3O_4 NPs integrated the local surface plasmon resonance (LSPR) characteristics of Au and the superparamagnetic properties of Fe_3O_4, which were used as new reporters in LFIA for *Salmonella typhimurium* detection. Au part provided favorable colorimetric signal due to its excellent LSPR characteristics. Fe_3O_4 part enabled magnetic separation and enrichment of the targets, improving the detection sensitivity and applicability in complex matrix. Besides, the Au-Fe_3O_4 NPs exhibited good photothermal effect due to the combination of Au and Fe_3O_4 [33–35]. By measuring the photothermal signal with a portable infrared thermal camera, accurate quantification of *S. typhimurium* was achieved. Thus, as new reporters, Au-Fe_3O_4 possessed multifunctions: target purification, target enrichment, and dual-mode detection (visual qualitation and instrumental quantification), which improved the limitations of traditional LFIA and showed great application potential in practice.

Experimental section

Reagents and instruments

Tetramethylammonium hydroxide (TMAH), Tween 20, polyvinylpyrrolidone (PVP, MW = 10,000), trisodium citrate (TSC), oleic acid, chloroauric acid ($HAuCl_4$), 1-octadecene, and iron pentacarbonyl were purchased from Macklin Biochemical Co., Ltd. HS-PEG-COOH (MW 2000) was bought from Shanghai ToYong Bio-Tech. Co., Ltd. Mouse anti-*S. typhimurium* monoclonal antibody was obtained from Abcam. *N*-(3-dimethylaminopropyl)-*N*′-ethylcarbodiimide hydrochloride (EDC), morpholino ethanesulfonic acid (MES), goat anti-mouse antibody, *N*-hydroxysuccinimide (NHS), acridine orange hemi (AO), and bovine serum albumin (BSA) were bought from Sigma-Aldrich. Heat-inactive *Escherichia coli*, *Listeria monocytogenes*, *S. typhimurium*, and *Staphylococcus aureus* were supplied by Army Medical University. Sample pad, conjugate pad, absorbent pad, nitrocellulose (NC) membrane, and PVC substrate were purchased from Joey-biotech Co., Ltd. Milk was bought from Nei Monggol Yili Industrial Group Co., Ltd. Ultrapure water was produced by a Millipore Milli-Q system.

Transmission electron microscopy (TEM) images were acquired by a microscope (JEOL, JEM 1400). High-resolution (HR) TEM and energy-dispersive X-ray (EDX) elemental mapping were obtained using a microscope (FEI, Tecnai F30). Absorption spectra were recorded with a spectrophotometer (Shimadzu, UV-2450). The test strips were sprayed by HGS510 (AUTOKUN) and divided by HGS210 induction cutting machine (AUTOKUN). Hydrodynamic diameters and zeta potentials were measured by a Zetasizer Nano ZS instrument (Malvern). Photothermal signals were collected by an infrared thermal camera (FOTRIC 226 s) mounted with an 808 laser (FU808AD2000-F34).

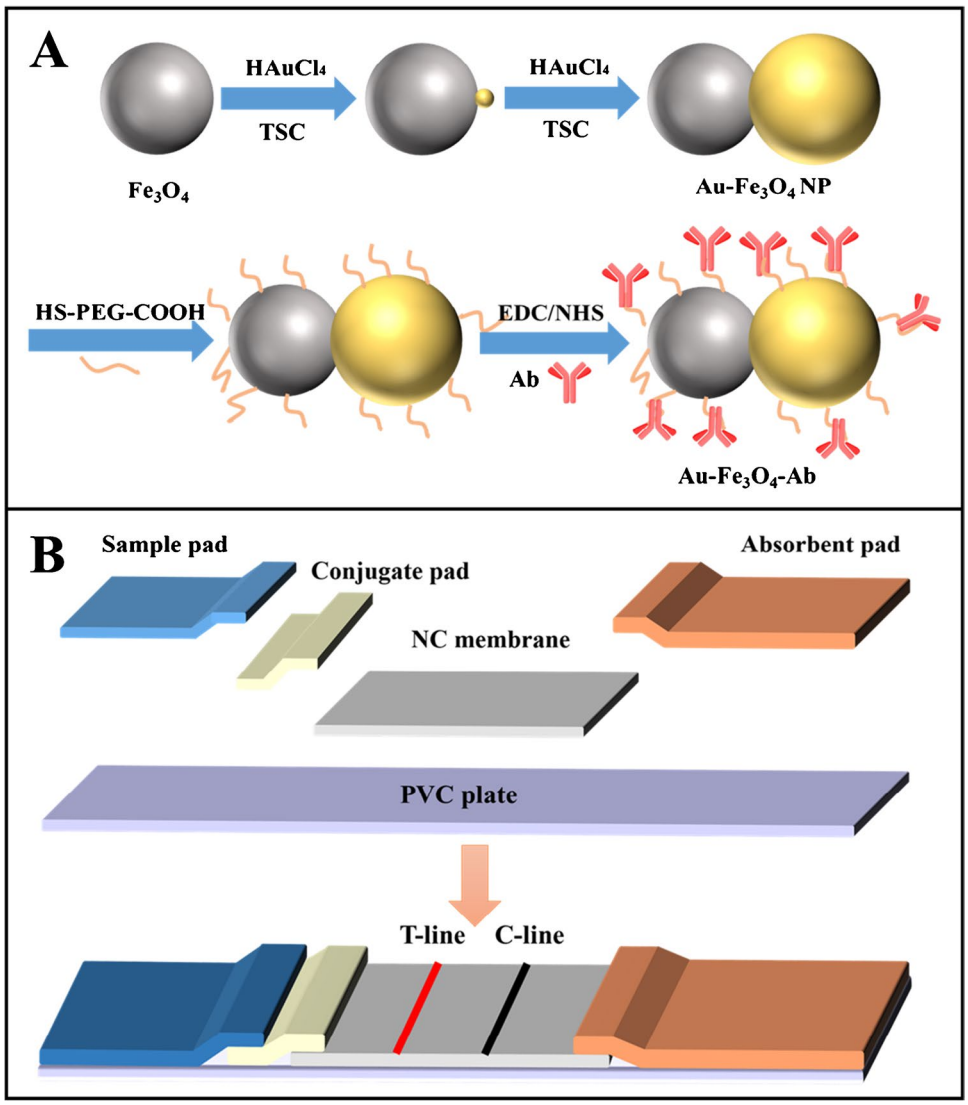

Scheme 1 **A** Schematic diagram for the preparation and modification of Au-Fe_3O_4 NPs. **B** Schematic diagram for the fabrication of LFIA strip

Magnetic separation was carried out with a magnet (Invitrogen, 12320D). The photographs were taken using iPhone11 (Apple).

Construction of anti-*S. typhimurium* antibody-modified Au-Fe_3O_4 NPs

Au-Fe_3O_4 heterodimer NPs were first prepared by seed-mediated approach referring to our previous work with slight modification [29]. Au^{3+} was reduced by Fe_3O_4, producing a gold seed on each Fe_3O_4 NP, which further grew by repeatedly adding TSC and Au precursor. The detail procedure was presented in the Supporting Information (S.1). Then, the biomodification of Au-Fe_3O_4 NPs was performed as follows.

Ten milliliters of Au-Fe_3O_4 NPs was added with 0.01 g of HS-PEG-COOH and shook for 1 h at 37 °C. Then, the above Au-Fe_3O_4 NPs were washed 3 times with 100 mM MES buffer (pH = 5.0) containing 0.05% Tween 20 and dispersed in 10 mL of MES buffer containing 2.5 mM NHS and 5 mM EDC. After 0.5 h reaction, the Au-Fe_3O_4 NPs were washed with PBS and dispersed in pH 7.2 PBS (0.01 M, 10 mL) to react with anti-*S. typhimurium* antibody (10 μg) for about 4 h. Finally, the obtained antibody-functionalized Au-Fe_3O_4 (Au-Fe_3O_4-Ab) NPs were washed 3 times by PBS, which were then blocked by 2% BSA, dispersed in 1 mL of PBS, and stored at 4 ℃. The complete preparation and modification process were illustrated in Scheme 1A.

Fabrication of LFIA strips

As illustrated in Scheme 1B, the test strip was constituted with sample pad, conjugate pad, NC membrane, and absorbent pad pasted onto the PVC plate. The overlap widths were about 2 mm between NC membrane and conjugate pad, 5 mm between NC membrane and absorbent pad, and 5 mm between conjugate pad and sample pad. Mouse anti-*S.*

typhimurium antibody (1.0 mg/mL) was sprayed at the T-line at a rate of 1.0 μL/cm. Goat anti-mouse antibody (1.0 mg/mL) was sprayed at the C-line at a rate of 1.0 μL/cm. Then, the strips were dried for 2 h at 37 °C, which were then cut into 3 mm width and kept in sealed plastic bag.

Detection of *S. typhimurium* with the dual-mode LFIA

In a typical test, 40 μL of Au-Fe_3O_4-Ab was added to 600 μL of test samples and incubated at 37 °C with gentle shaking. Then, the mixture was separated by a magnet and resuspended with a solution containing 70 μL of pH 7.2 PBS, 10 μL of Au-Fe_3O_4-Ab, and 20 μL of running solution (2.0% BSA and 0.25% Tween 20 in pH 7.2 PBS). The above solution was transferred to a microtiter plate and the sample pad of the LFIA strip was immersed in it. All the liquid was absorbed and migrated along the strip. After 15 min, by observing T-line color with the naked eyes, qualitative detection was achieved. Meanwhile, the photothermal signal of the T-line was measured for quantitative detection, which was defined as follows.

$$\Delta T = \Delta T_1 - \Delta T_0$$

where ΔT_1 was the temperature variation of the tested strips before and after irradiation and ΔT_0 was the temperature variation of the unused strips.

Detection of *S. typhimurium* in simulated complex samples

The whole milk was first tested by PCR methods to certify that they were not contaminated by *S. typhimurium* as our previous work [36]. Then, the milk was mixed with *S. typhimurium* suspension in 0.1 M pH 7.2 PBS (9:1 by volume) to simulate complex samples. For detection, Au-Fe_3O_4-Ab was added to incubate with the simulated samples. After the reaction, separation, and immunochromatography with the dual-mode strip as described in the previous section, naked-eye observing and photothermal signal measuring were performed. Blank milk samples were treated the same except no bacterium was added. Meanwhile, PBS samples with the same bacteria concentrations were detected for control.

Results and discussion

Principle of the dual-mode LFIA for detecting *S. typhimurium*

As illustrated by Fig. 1A, Au-Fe_3O_4-Ab was first added to the samples to capture and separate *S. typhimurium*. This step achieved enrichment and purification of target bacteria, which would greatly facilitate enhancing detection signal and reducing interference. Then, the obtained Au-Fe_3O_4-Ab-*S. typhimurium* complexes were loaded on the LFIA strip, which were captured by the anti-*S. typhimurium* antibody on the T-line, inducing a colored band. Free Au-Fe_3O_4-Ab migrated further, which were captured by the anti-mouse antibody on the C-line to produce a quality control band. For negative samples without *S. typhimurium*, Au-Fe_3O_4-Ab would flow past the T-line without interaction and only react with the C-line. Thus, as illustrated in Fig. 1B, positive samples produced both colored C-line and T-line, and negative samples only produced colored C-line. While for the ones whose C-line did not show color, indicating the antibody had lost bioactivity, the results were invalid. By observing the color bands with the naked eyes, qualitative detection was performed free of instrument. Meanwhile, by measuring the photothermal signal of the T-line with a portable infrared thermal camera, quantification was achieved. Figure 1B also

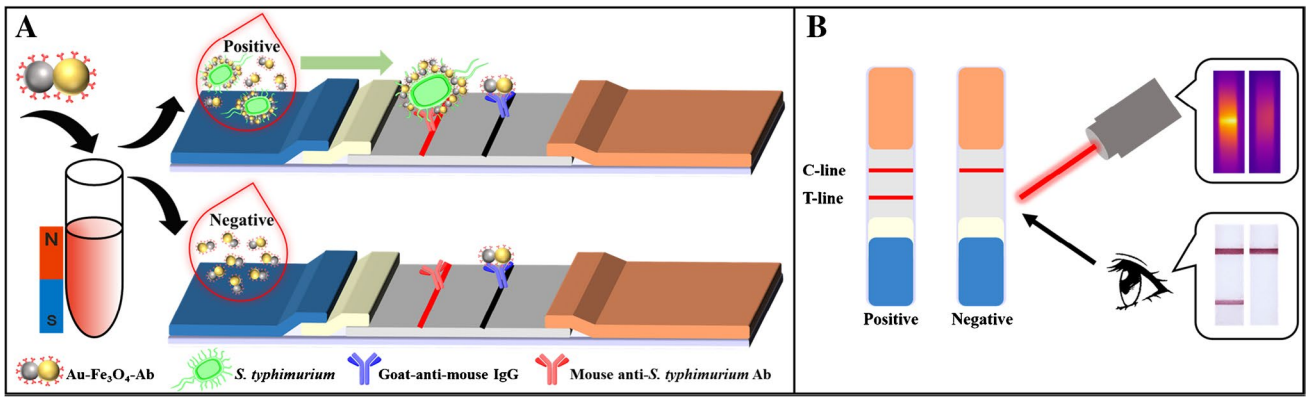

Fig. 1 **A** Schematic diagram for *S. typhimurium* detection with the dual-mode LFIA. **B** Interpretation of the detection results and the typical positive and negative results from visual and infrared thermal camera observation

shows the typical positive and negative results from visual and thermal camera observation. It could be seen that the positive one showed two clear colored bands, and its T-line produced an obvious high temperature zone. While for the negative one, only the C-line produced color, and the temperature of its T-line hardly rose.

Characterization of Au-Fe_3O_4 and Au-Fe_3O_4-Ab NPs

As shown in Fig. 2A-B, Au-Fe_3O_4 NPs possessed good dispersion with an average size of 35.6 ± 2.3 nm (200 particles were counted for calculation) and mainly exhibited one-to-one dumbbell structure. From the EDX elemental mapping of one single NP (Fig. 2C–E), it could be seen that Fe element and Au element were respectively distributed in the two sections of the heterodimer, which further confirmed its structure. Besides, the Au-Fe_3O_4 solution showed a wine-red color with a maximum absorbance peak at 522 nm (Fig. 2F).

For construction of Au-Fe_3O_4-Ab, carboxyl groups were first introduced on Au-Fe_3O_4 NP surface with HS-PEG-COOH based on coordination interaction and then conjugated with the amino groups of anti-*S. typhimurium* antibody through carbodiimide chemistry. The Au-Fe_3O_4-Ab remained the optical and morphology properties of Au-Fe_3O_4 NPs. As shown in Fig. 2F–G, Au-Fe_3O_4-Ab NPs had good dispersibility with an average size of 37.0 ± 2.3 nm (200 particles were counted for calculation) and exhibited a wine-red color with a maximum absorbance peak at 528 nm, which only slightly changed compared with Au-Fe_3O_4 NPs. To confirm the conjugation, the hydrodynamic diameter and zeta potential of the NPs before and after functionalization were measured, and the results are shown in Fig. 2H. It could be seen that the hydrodynamic diameter produced an obvious increase from 76 to 150 nm, and the zeta potential changed from − 66 to − 16 mV, which demonstrated the antibody was successfully coupled with the NPs [37–39]. Furthermore, Au-Fe_3O_4 and Au-Fe_3O_4-Ab were, respectively, loaded on the LFIA strips, and as shown in Fig. 2I, the strip with Au-Fe_3O_4-Ab produced a colored C-line, while the strip with Au-Fe_3O_4 produced no colored line. This demonstrated that the anti-*S. typhimurium* antibody on the NPs maintained good bioactivity, which could react with the goat anti-mouse antibody on the C-line.

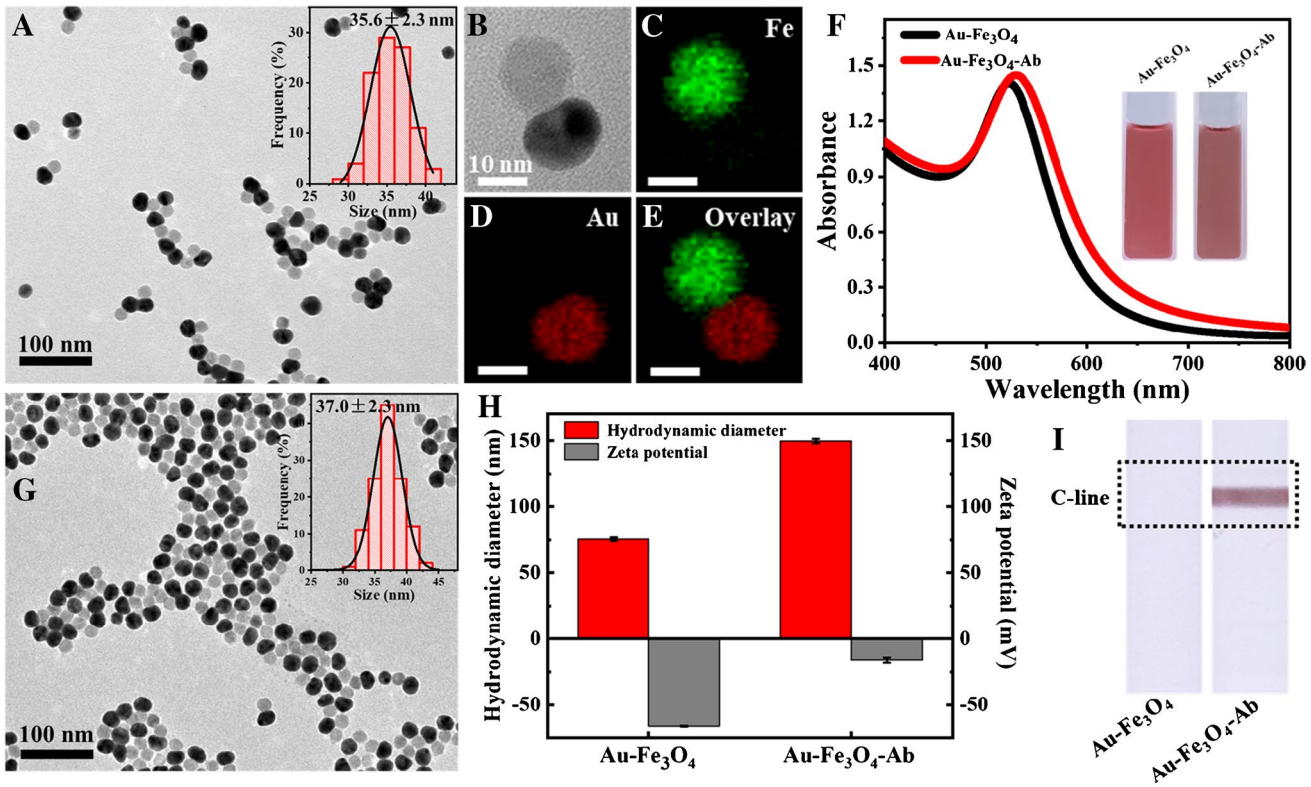

Fig. 2 Characterization of Au-Fe_3O_4 and Au-Fe_3O_4-Ab NPs. **A** TEM image and size distribution of Au-Fe_3O_4 NPs. **B** HR-TEM image of a single Au-Fe_3O_4 NP. **C–E** EDX element mappings of Fe, Au, and the overlay. **F** UV–Vis spectra of Au-Fe_3O_4 and Au-Fe_3O_4-Ab solution and the corresponding photos (inset). **G** TEM image and size distribution of Au-Fe_3O_4-Ab NPs. **H** Hydrodynamic diameters and zeta potentials of Au-Fe_3O_4 and Au-Fe_3O_4-Ab. **I** Photographs of the test strips loaded with Au-Fe_3O_4 and Au-Fe_3O_4-Ab NPs

Reliability of the dual-mode LFIA

Fluorescence microscopy and TEM analyses were performed to investigate the capture of *S. typhimurium* with Au-Fe_3O_4-Ab. From Fig. 3A, it can be seen that many green fluorescence dots, indicating AO-stained bacteria, could be found after the capture of *S. typhimurium* by Au-Fe_3O_4-Ab. While using Au-Fe_3O_4 to treat *S. typhimurium*, no bacterium was observed (Fig. S1A). This demonstrated that Au-Fe_3O_4-Ab could efficiently capture *S. typhimurium* based on antibody-antigen interaction. TEM image more intuitively showed the combination between *S. typhimurium* and Au-Fe_3O_4-Ab. From Fig. 3B, it can be seen that many Au-Fe_3O_4-Ab NPs bound with the bacterium surfaces. While using Au-Fe_3O_4 to treat *S. typhimurium*, few NPs combined with *S. typhimurium*, and after separation, only Au-Fe_3O_4 NPs were observed rather than bacteria (Fig. S1B-C). This matched well with the microscopy analyses.

Then, we explored the effect of magnetic enrichment on detection signal. As shown in Fig. 3C, compared with the samples without enrichment, the enriched ones achieved higher photothermal signals, facilitating enhanced detection sensitivity. Besides, the magnetic attraction time in separation also influenced the detection signal, due to the fact that the attraction time affected the capture efficiency. With the increase of attraction time, the signals from positive samples and negative ones both increased, and 15 min induced the highest signal-to-noise ratio (the ratio of the positive sample signal to the negative sample signal), which was chosen as the optimal attraction time. Other conditions, including irradiation power density, irradiation time, amount of Au-Fe_3O_4-Ab NPs, and incubation time, were also optimized. Finally, 4 W/cm^2, 100 s irradiation, 40 μL of Au-Fe_3O_4-Ab NPs, and 20-min incubation were selected (Fig. S2-5).

Under optimal conditions, the specificity and reproducibility of the dual-mode LFIA were evaluated. *S. typhimurium*, *L. monocytogenes*, *S. aureus*, and *E. coli* at the same concentration (5×10^7 CFU/mL) and the blank samples without bacteria were detected by the strips. As shown in Fig. 3D, *S. typhimurium* samples produced obvious colored T-line and strong photothermal signal, while other bacteria showed similar phenomenon as that of the blank, in which no colored T-line or obvious photothermal signal was found. Meanwhile, we calculated the coefficient of variations of the intra-assay and inter-assay as 3.0% and 7.9%, confirming the good reproducibility.

All the above results demonstrated that this Au-Fe_3O_4 multifunctional NPs-based LFIA enabled efficient capture of *S. typhimurium*, and the pre-enrichment enhanced the detection signal, definitely improving the sensitivity. Besides, this LFIA had good specificity and reproducibility, assuring the detection reliability.

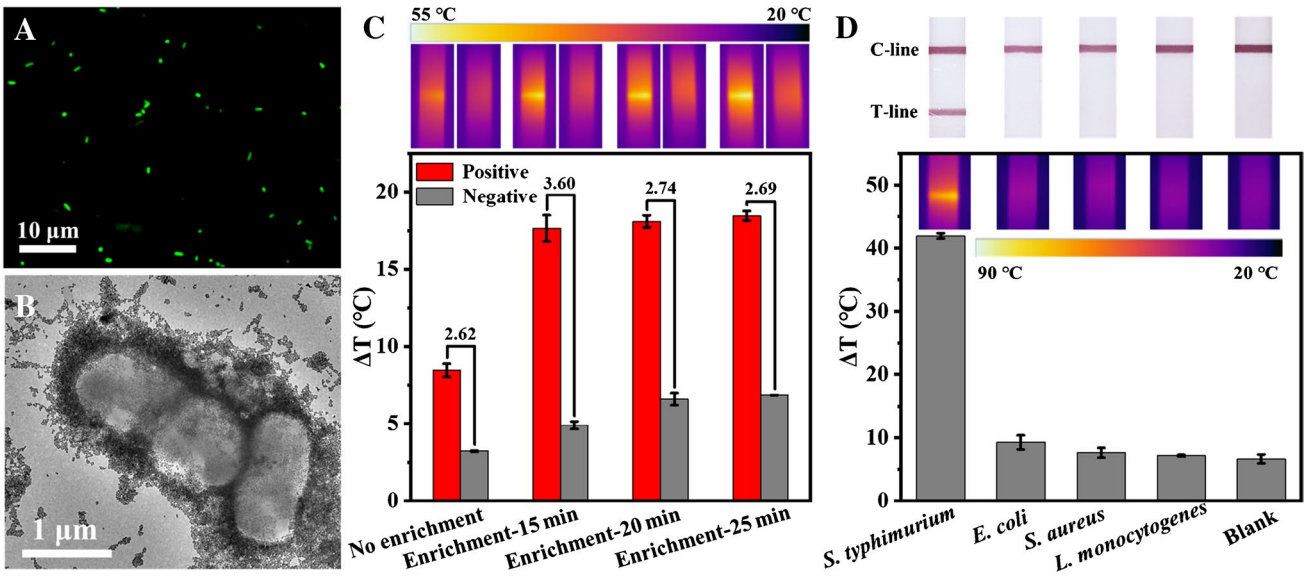

Fig. 3 **A**–**B** Fluorescence microscopic image and TEM image of *S. typhimurium* captured by Au-Fe_3O_4-Ab. **C** Photothermal signals obtained from positive samples (1×10^7 CFU/mL *S. typhimurium*) and blank samples enriched by different magnetic attraction times. The lower is the histogram of photothermal signals, the upper are the corresponding photothermal images. The numbers above the columns are the signal-to-noise ratios. **D** Results from detection of different bacteria (5×10^7 CFU/mL). The lower is the photothermal signal histogram and images of the test strips, the upper are the corresponding photographs by phones. Error bars are calculated from three experiments

Analytical performance of the LFIA

To evaluate the sensitivity and dynamic range, the dual-mode LFIA was used to detect different concentrations of *S. typhimurium*. As shown in Fig. 4A, for the negative samples, only the C-line generated a colored band, and when the *S. typhimurium* concentration reached 5×10^5 CFU/mL, the T-line began to display a visible color. As the bacteria concentration increased further, the T-line color became darker, due to the fact that more Au-Fe_3O_4-Ab-*S. typhimurium* complexes were accumulated on the test zone. Therefore, by observing the color change of the T-line with the naked eyes, qualitative detection of *S. typhimurium* was achieved with a limit of 5×10^5 CFU/mL. Meanwhile, the photothermal signals of the strips were measured, which are shown in Fig. 4B. Similar with the visual detection, the photothermal signal increased with the bacteria concentration. According to the lowest distinguishable signal ($S_{blank}+3SD$, where S_{blank} is the average signal of blank groups, and SD is their standard deviation), the limit of the photothermal detection could achieve 5×10^4 CFU/mL, which was one order of magnitude lower than that of the visual observing. Moreover, a good linear relationship was exhibited at the concentration from 5×10^6 to 1×10^8 CFU/mL with $R^2 = 0.9989$ (Fig. 4C), facilitating accurate quantification of *S. typhimurium*. Compared with the commercial LFIA [27], this dual-mode LFIA increased the sensitivity by 1–2 orders of magnitude, which might be attributed to the pre-enrichment of the target bacteria.

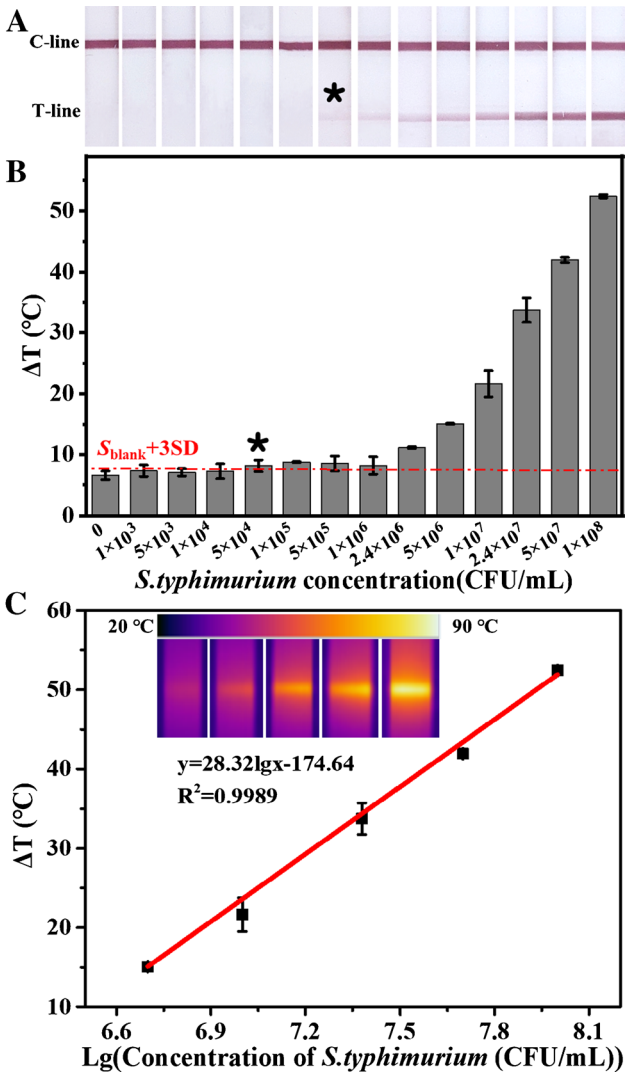

Fig. 4 **A**–**B** Photographs of the test strips and the corresponding photothermal signals obtained from detection of different concentrations of *S. typhimurium*. The asterisk represents the detection limit. The red line represents the lowest distinguishable signal by photothermal measuring. **C** Calibration plot of photothermal signal *versus S. typhimurium* concentration. The insets are the corresponding photothermal images. Error bars are calculated from three experiments

Application to simulated complex samples

To test the feasibility of the dual-mode LFIA in complex biological matrixes, unprocessed milk spiked with *S. typhimurium* was used to mimic real samples for detection. As shown in Fig. 5, all the positive milk samples produced two obvious colored bands, and the negative one only produced a colored C-line, which were almost the same with those of the buffer samples. By measuring the photothermal

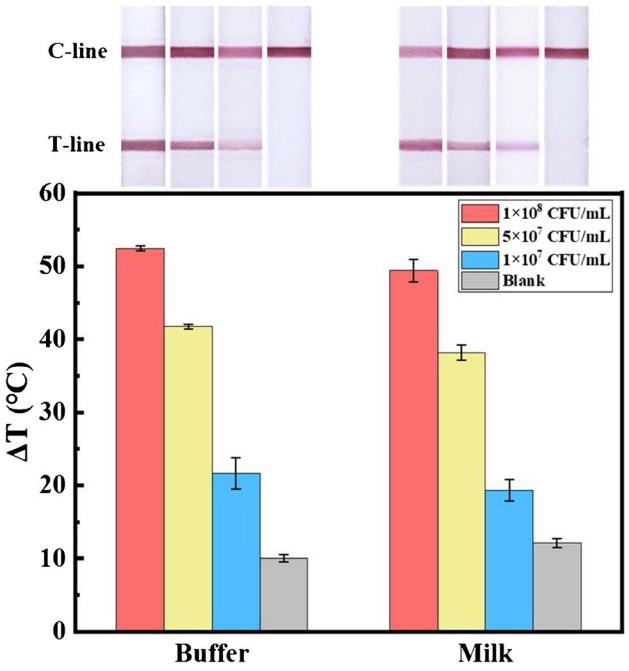

Fig. 5 Photothermal signal histograms of the test strips and their corresponding photographs obtained from detecting different concentrations of *S. typhimurium* in buffer and milk samples. Error bars are calculated from three experiments

Table 1 An overview on recently reported LFIA for detection of *Salmonella*

Materials used	Signal	Detection limit (CFU/mL)	Assay time	Linearity range (CFU/mL)	Complex samples	Ref
Gold nanoparticles	Color	10^7	30 min	Qualitative		[40]
Gold-coated gold nanoparticles	Color	10^4	20 min	Qualitative	Diluted fat-reduced milk	[41]
Nitrogen-rich carbon nanoparticles	Color	10^2	20 min	10^2–10^8	Diluted juice and vegetable salad	[42]
Au@Ru nanocomposites	Color	9.8×10^4	10 min	2.9×10^6–2.9×10^{11}	Diluted drinking water, juice, and milk	[39]
Quantum dot nanobeads	Fluorescence	5×10^3	12 min	5×10^4–10^7	Broth processed by centrifugation	[43]
Up-converting phosphor	Fluorescence	10^4	20 min	10^4–10^7	Food samples cultured for about 14 h	[44]
Magnetic nanoparticles	Color	1.95×10^5	30 min	Qualitative	Low fat milk	[45]
Fluorescent-magnetic nanospheres	Fluorescence and magnetic signal	3.5×10^3	35 min	1.88×10^4–1.88×10^7	Milk, serum, and whole blood	[27]
Au-Fe_3O_4 nanoparticles	Color and photothermal signal	5×10^4	50 min	5×10^6–1×10^8	Whole milk	This work

signal, the milk samples induced slightly lower signal than the buffer samples, and the recovery was $72.70\pm8.28\%$ (Table S1), which was tolerable, due to the complexity of the unprocessed milk, while the commercial LFIA can be only applied to diluted milk, because the unprocessed milk cannot migrate on strips. This dual-mode LFIA's better analytical performance in complex matrixes was mainly attributed to the pre-enrichment and pre-purification by magnetic separation, which made it possess great potential application in practice.

Conclusions

In this work, we directly synthesized Au-Fe_3O_4 multifunctional NPs and integrated them with LFIA as promising alternative reporters for dual-mode detection of *S. typhimurium*. Table 1 shows the analytical performance comparison between this dual-mode LFIA with other recently reported LFIA. It can be seen that this dual-mode LFIA indeed improved the limitations of traditional LFIA (Au-based LFIA) [40], and it increased the detection sensitivity by 2 orders of magnitude. Moreover, compared with carbon nanoparticles, quantum dots, up-converting materials, etc. [39, 41–44], Au-Fe_3O_4 NPs enabled enrichment and purification of target bacteria from complex matrix, thus achieving direct application to unprocessed whole milk. Besides, Au-Fe_3O_4 NPs could provide photothermal signal, facilitating quantitative detection with a portable infrared thermal camera, which was more sensitive than color observing and more cost-effective than fluorescence or magnetic signal determination [27, 45]. However, there is still room for improvement in this method. In the future, we will try to optimize the Fe_3O_4 size and the Au absorption to obtain faster enrichment and better photothermal signal and then make the manipulation more convenient and achieve more sensitive detection.

Supplementary Information The online version contains supplementary material available at https://doi.org/10.1007/s00604-023-05645-x.

Funding This work was financially supported by the Natural Scientific Foundation of Shandong (ZR2020MB064, ZR2020ZD13, ZR2022JQ07), the Science and Technology Projects of Qingdao (21–1-4-sf-7-nsh), the National Natural Science Foundation of China (No. 21876206), and the Fundamental Research Funds for the Central Universities (No. 22CX03033A).

Data availability Date will be made available on request.

Declarations

Conflict of interest The authors declare no competing interests.

References

1. WHO Fact Sheets: Food Safety - the Global View, http://www.who.int/mediacentre/factsheets/fs399/en/, accessed: July 2022
2. Shen Y, Zhang Y, Gao ZF, Ye Y, Wu Q, Chen H-Y, Xu J-J (2021) Recent advances in nanotechnology for simultaneous detection of multiple pathogenic bacteria. Nano Today 38:101121. https://doi.org/10.1016/j.nantod.2021.101121
3. Furst AL, Francis MB (2019) Impedance-based detection of bacteria. Chem Rev 119(1):700–726. https://doi.org/10.1021/acs.chemrev.8b00381
4. Liu J, Bai L, Li W, Han H, Fu P, Ma X, Bi Z, Yang X, Zhang X, Zhen S, Deng X, Liu X, Guo Y (2018) Trends of foodborne diseases in China: lessons from laboratory-based surveillance

since 2011. Front Med 12(1):48–57. https://doi.org/10.1007/s11684-017-0608-6
5. Lu Z, Liu W, Cai Y, Zhao T, Cui M, Zhang H, Du S (2022) Salmonella typhimurium strip based on the photothermal effect and catalytic color overlap of PB@Au nanocomposite. Food Chem 385:132649. https://doi.org/10.1016/j.foodchem.2022.132649
6. Varadi L, Luo JL, Hibbs DE, Perry JD, Anderson RJ, Orenga S, Groundwater PW (2017) Methods for the detection and identification of pathogenic bacteria: past, present, and future. Chem Soc Rev 46(16):4818–4832. https://doi.org/10.1039/c6cs00693k
7. Chang D, Zakaria S, Esmaeili Samani S, Chang Y, Filipe CDM, Soleymani L, Brennan JD, Liu M, Li Y (2021) Functional nucleic acids for pathogenic bacteria detection. Acc Chem Res 54(18):3540–3549. https://doi.org/10.1021/acs.accounts.1c00355
8. Wei L, Wang Z, Feng C, Xianyu Y, Chen Y (2021) Direct transverse relaxation time biosensing strategy for detecting foodborne pathogens through enzyme-mediated sol-gel transition of hydrogels. Anal Chem 93(17):6613–6619. https://doi.org/10.1021/acs.analchem.0c03968
9. Qi X, Wang Z, Lu R, Liu J, Li Y, Chen Y (2021) One-step and DNA amplification-free detection of Listeria monocytogenes in ham samples: combining magnetic relaxation switching and DNA hybridization reaction. Food Chem 338:127837. https://doi.org/10.1016/j.foodchem.2020.127837
10. Bahadır EB, Sezgintürk MK (2016) Lateral flow assays: principles, designs and labels. TrAC-Trend Anal Chem 82:286–306. https://doi.org/10.1016/j.trac.2016.06.006
11. Parolo C, Sena-Torralba A, Bergua JF, Calucho E, Fuentes-Chust C, Hu L, Rivas L, Alvarez-Diduk R, Nguyen EP, Cinti S, Quesada-Gonzalez D, Merkoci A (2020) Tutorial: design and fabrication of nanoparticle-based lateral-flow immunoassays. Nat Protoc 15(12):3788–3816. https://doi.org/10.1038/s41596-020-0357-x
12. Chen X, Ding L, Huang X, Xiong Y (2022) Tailoring noble metal nanoparticle designs to enable sensitive lateral flow immunoassay. Theranostics 12(2):574–602. https://doi.org/10.7150/thno.67184
13. The history of the pregnancy test, https://history.nih.gov/exhibits/thinblueline/timeline.htm#1970, accessed: July 2022
14. Bhalla N, Pan Y, Yang Z, Payam AF (2020) Opportunities and challenges for biosensors and nanoscale analytical tools for pandemics: COVID-19. ACS Nano 14(7):7783–7807. https://doi.org/10.1021/acsnano.0c04421
15. Zhong Y, Chen Y, Yao L, Zhao D, Zheng L, Liu G, Ye Y, Chen W (2016) Gold nanoparticles based lateral flow immunoassay with largely amplified sensitivity for rapid melamine screening. Microchim Acta 183(6):1989–1994. https://doi.org/10.1007/s00604-016-1812-9
16. Sohrabi H, Majidi MR, Khaki P, Jahanban-Esfahlan A, de la Guardia M, Mokhtarzadeh A (2022) State of the art: lateral flow assays toward the point-of-care foodborne pathogenic bacteria detection in food samples. Comp Rev Food Sci Food Saf 21(2):1868–1912. https://doi.org/10.1111/1541-4337.12913
17. Zhang C, Wang Y, Liu Z, Bai M, Wang J, Wang Y (2022) Nanobody-based immunochromatographic biosensor for colorimetric and photothermal dual-mode detection of foodborne pathogens. Sensors and Actuators B: Chemical 369:132371. https://doi.org/10.1016/j.snb.2022.132371
18. Fan LZ, Yang J, Wu JB, Li FG, Yan WN, Tan F, Zhang M, Draz MS, Han HX, Zhang PF (2022) Deeply-dyed nanobead system for rapid lateral flow assay testing of drugs at point-of-care. Sensors and Actuators B-Chemical 362. https://doi.org/10.1016/j.snb.2022.131829
19. Zheng P, Peng T, Wang J, Zhang J, Wang Z, Zhang Y, Ren Z, Wang S, Jiang H (2021) Fluorescent lateral flow immunoassay based on gold nanocluster for detection of pyrrolizidine alkaloids. Microchim Acta 188(1):11. https://doi.org/10.1007/s00604-020-04672-2
20. Liang P, Guo Q, Zhao T, Wen CY, Tian Z, Shang Y, Xing J, Jiang Y, Zeng J (2022) Ag nanoparticles with ultrathin Au shell-based lateral flow immunoassay for colorimetric and SERS dual-mode detection of SARS-CoV-2 IgG. Anal Chem 94(23):8466–8473. https://doi.org/10.1021/acs.analchem.2c01286
21. Qiu W, Baryeh K, Takalkar S, Chen W, Liu G (2019) Carbon nanotube-based lateral flow immunoassay for ultrasensitive detection of proteins: application to the determination of IgG. Microchim Acta 186(7):436. https://doi.org/10.1007/s00604-019-3508-4
22. Iranmanesh M, Hulliger J (2017) Magnetic separation: its application in mining, waste purification, medicine, biochemistry and chemistry. Chem Soc Rev 46(19):5925–5934. https://doi.org/10.1039/c7cs00230k
23. Xiao D, Lu T, Zeng R, Bi Y (2016) Preparation and highlighted applications of magnetic microparticles and nanoparticles: a review on recent advances. Microchim Acta 183(10):2655–2675. https://doi.org/10.1007/s00604-016-1928-y
24. Wang Z, Cai R, Gao Z, Yuan Y, Yue T (2020) Immunomagnetic separation: an effective pretreatment technology for isolation and enrichment in food microorganisms detection. Compr Rev Food Sci Food Saf 19(6):3802–3824. https://doi.org/10.1111/1541-4337.12656
25. Wang Z, Xianyu Y, Zhang Z, Guo A, Li X, Dong Y, Chen Y (2019) Background signal-free magnetic bioassay for food-borne pathogen and residue of veterinary drug via Mn(VII)/Mn(II) interconversion. ACS Sens 4(10):2771–2777. https://doi.org/10.1021/acssensors.9b01349
26. Hwang J, Kwon D, Lee S, Jeon S (2016) Detection of Salmonella bacteria in milk using gold-coated magnetic nanoparticle clusters and lateral flow filters. RSC Adv 6(54):48445–48448. https://doi.org/10.1039/c6ra05446c
27. Hu J, Jiang YZ, Tang M, Wu LL, Xie HY, Zhang ZL, Pang DW (2019) Colorimetric-fluorescent-magnetic nanosphere-based multimodal assay platform for Salmonella detection. Anal Chem 91(1):1178–1184. https://doi.org/10.1021/acs.analchem.8b05154
28. Wang C, Shen W, Rong Z, Liu X, Gu B, Xiao R, Wang S (2020) Layer-by-layer assembly of magnetic-core dual quantum dot-shell nanocomposites for fluorescence lateral flow detection of bacteria. Nanoscale 12(2):795–807. https://doi.org/10.1039/c9nr08509b
29. Zeng J, Gong M, Wang D, Li M, Xu W, Li Z, Li S, Zhang D, Yan Z, Yin Y (2019) Direct synthesis of water-dispersible magnetic/plasmonic heteronanostructures for multimodality biomedical imaging. Nano Lett 19(5):3011–3018. https://doi.org/10.1021/acs.nanolett.9b00171
30. Dong Y, Wen CY, She Y, Zhang Y, Chen Y, Zeng J (2021) Magnetic relaxation switching immunoassay based on hydrogen peroxide-mediated assembly of Ag@Au-Fe3 O4 nanoprobe for detection of aflatoxin B1. Small:e2104596. https://doi.org/10.1002/smll.202104596
31. Qiu Z, Duan W, Cao S, Zeng T, Zhao T, Huang J, Lu X, Zeng J (2022) Highly specific colorimetric probe for fluoride by triggering the intrinsic catalytic activity of a AgPt-Fe3O4 hybrid nanozyme encapsulated in SiO2 shells. Environ Sci Technol 56(3):1713–1723. https://doi.org/10.1021/acs.est.1c06453
32. Zhang Y, Gong M, Li X, Liu H, Liang P, Cui S, Zhang L, Zhou C, Sun T, Zhang M, Wen C-Y, Zeng J (2022) Au-Fe3O4 heterodimer multifunctional nanoparticles-based platform for ultrasensitive naked-eye detection of Salmonella typhimurium. J Hazard Mater 436:129140. https://doi.org/10.1016/j.jhazmat.2022.129140
33. Feng W, Zhou X, Nie W, Chen L, Qiu K, Zhang Y, He C (2015) Au/polypyrrole@Fe3O4 nanocomposites for MR/CT dual-modal imaging guided-photothermal therapy: an in vitro study. ACS Appl Mater Interfaces 7(7):4354–4367. https://doi.org/10.1021/am508837v
34. Yang Z, Ding X, Jiang J (2016) Facile synthesis of magnetic–plasmonic nanocomposites as T 1 MRI contrast enhancing and

photothermal therapeutic agents. Nano Res 9(3):787–799. https://doi.org/10.1007/s12274-015-0958-9
35. Wang S, Hou Y (2021) Photothermal therapy based on magnetic nanoparticles in cancer. J Appl Phys 130(7):070902. https://doi.org/10.1063/5.0057671
36. Wen CY, Hu J, Zhang ZL, Tian ZQ, Ou GP, Liao YL, Li Y, Xie M, Sun ZY, Pang DW (2013) One-Step sensitive detection of Salmonella typhimurium by coupling magnetic capture and fluorescence identification with functional nanospheres. Anal Chem 85(2):1223–1230. https://doi.org/10.1021/ac303204q
37. Liu J, Lin L, Yao P, Zhao W, Hu J, Shi XH, Zhang S, Zhu X, Pang DW, Liu AA (2022) Immunoprofiling of severity and stage of bacterial infectious diseases by ultrabright fluorescent nanosphere-based dyad test strips. Anal Chem 94(24):8818–8826. https://doi.org/10.1021/acs.analchem.2c02028
38. Yu X, Xia HS, Sun ZD, Lin Y, Wang K, Yu J, Tang H, Pang DW, Zhang ZL (2013) On-chip dual detection of cancer biomarkers directly in serum based on self-assembled magnetic bead patterns and quantum dots. Biosens Bioelectron 41:129–136
39. Ji L, Zhang L, Yang H, Liang S, Pan J, Zou Y, Li S, Li Q, Zhao S (2022) Versatile Au@Ru nanocomposites for the rapid detection of Salmonella typhimurium and photothermal sterilization. J Colloid Interface Sci 621:489–498. https://doi.org/10.1016/j.jcis.2022.04.028
40. Liu CC, Yeung CY, Chen PH, Yeh MK, Hou SY (2013) Salmonella detection using 16S ribosomal DNA/RNA probe-gold nanoparticles and lateral flow immunoassay. Food Chem 141(3):2526–2532. https://doi.org/10.1016/j.foodchem.2013.05.089
41. Bu T, Huang Q, Yan L, Huang L, Zhang M, Yang Q, Yang B, Wang J, Zhang D (2018) Ultra technically-simple and sensitive detection for Salmonella enteritidis by immunochromatographic assay based on gold growth. Food Control 84:536–543. https://doi.org/10.1016/j.foodcont.2017.08.036
42. Wang Z, Yao X, Wang R, Ji Y, Yue T, Sun J, Li T, Wang J, Zhang D (2019) Label-free strip sensor based on surface positively charged nitrogen-rich carbon nanoparticles for rapid detection of Salmonella enteritidis. Biosens Bioelectron 132:360–367. https://doi.org/10.1016/j.bios.2019.02.061
43. Hu J, Tang F, Jiang YZ, Liu C (2020) Rapid screening and quantitative detection of Salmonella using a quantum dot nanobead-based biosensor. Analyst 145(6):2184–2190. https://doi.org/10.1039/d0an00035c
44. Zhao Y, Wang H, Zhang P, Sun C, Wang X, Wang X, Yang R, Wang C, Zhou L (2016) Rapid multiplex detection of 10 foodborne pathogens with an up-converting phosphor technology-based 10-channel lateral flow assay. Sci Rep 6:21342. https://doi.org/10.1038/srep21342
45. Duan M-L, Huang Y-M, Wu S-S, Li G-Q, Wang S-Y, Chen M-H, Wang C, Liu D-F, Liu C-W, Lai W-H (2017) Rapid and sensitive detection of Salmonella enteritidis by a pre-concentrated immunochromatographic assay in a large-volume sample system. RSC Adv 7(87):55141–55147. https://doi.org/10.1039/c7ra11006e